Electronic Supplementary Material (ESI) for Journal of Materials Chemistry C.
This journal is © The Royal Society of Chemistry 2017

Supplementary Information for Rational Design of Transparent P-type Conducting Non-oxide Materials From High-throughput Calculations

K. R. Ramya, Thomas D. Khne, Claudia Felser, and Hossein Mirhosseini

December 8, 2017

1 Thermodynamic limits of dopants chemical potentials

When dopants are incorporated into the host semiconductor, depending on experimental conditions, the chemical potentials of the dopants are subjected to specific bounds. In our calculations, we considered two extreme limits, namely when the dopants are in the elemental phase, and when the chemical potentials of dopants are bounded by avoiding the formation of the secondary phases. Various secondary phases that may form in the presence of the dopants are listed in Table 1. In Table 2, we listed the thermodynamic limits for the chemical potential of dopants to avoid the formation of the secondary phases. Figure 1 shows the formation energies under the former condition (dopants in the elemental phase). The formation energies under later condition are shown in the manuscript.

Table 1: Calculated formation energies of various phases which determine the stability regions of each compound and the maximum chemical potential of dopants.

Compound	Formation energy (eV)	Compound	Formation energy (eV)
BeTe	-0.75	KS	-1.88
Be_3N_2	-12.85	KZn_{13}	-0.61
Li_2Se	-3.81	GaSe	-1.21
LiZn	-0.42	GaTe	-0.74
$LiZn_3$	-0.52	Ga_2Se_3	-1.94
Li_2Te	-3.14	$GaSe_2$	-0.04
Na_2S	-3.38	GaP	-0.83
Na_2S_5	-3.54	Ga_2Te_3	-2.02
NaS	-1.70	Ga_2Te_5	-1.70
NaS_2	-1.78	Ga_7Te_{10}	-5.79
NaSe	-1.69	GaN	-4.60
$NaSe_2$	-1.74	ZnSe	-1.41
Na_2Te	-2.85	ZnTe	-0.92
$NaTe_3$	-1.57	ZnS	-1.60
Na_2Te	-2.83	$Zn(GaSe_2)_2$	-4.57
$NaTe_3$	-1.57	$Zn(GaTe_2)_2$	-2.69
Na_2ZnS_2	-4.99	Zn_3N_2	-5.97
Na_6ZnS_4	-11.68	Zn_8Cu_5	-1.19
$NaZn_{13}$	-0.39	Zn_3P_2	-0.94
$Na_2Ge_2S_5$	-6.07	ZnP_2	-0.77
Na_2GeS_3	-5.08	MgS	-2.87
$Na_6Ge_2S_7$	-18.50	MgTe	-1.66
NaGe	-0.34	Mg_3N_2	-11.26
Na_2ZnSe_2	-4.73	$Mg_{17}Al_{12}$	-0.94
$Na_4Zn_3Se_5$	-10.89	$Mg_{23}Al_{30}$	-1.84
Na_6ZnSe_4	-11.35	Al_2Se_3	-4.23
$NaZn_{13}$	-0.39	AlN	-6.49
K_2Se	-3.15	GeS	-0.52
K_2Se_3	-3.86	Ge_3N_4	-14.55
K_2Se_5	-3.91	CuTe	-0.18
KSe	-1.81	Cu_3Se_2	-0.74
K_2Te	-3.09	CuSe	-0.29
K_2Te_3	-3.56	$CuSe_2$	-0.28
KTe	-1.68	SN	-2.57
K_2S	-3.01	S_2N	-2.40
K_2S_3	-3.99	PSe	-0.19
K_2S_5	-4.14		

Table 2: The thermodynamic limits of the chemical potential of dopants in anion-rich conditions.

Compound	$\Delta\mu_{\rm i}$ (eV)
ZnS	$\Delta\mu_{\rm Na}$ = -1.79, $\Delta\mu_{\rm K}$ = -2.00, $\Delta\mu_{\rm N}$ = -0.58
ZnSe	$\Delta\mu_{\rm Li}$ = -1.90, $\Delta\mu_{\rm Na}$ = -1.74
ZnTe	$\Delta\mu_{\rm Na}$ = -1.56, $\Delta\mu_{\rm Cu}$ = -0.18, $\Delta\mu_{\rm N}$ = -1.60
MgS	$\Delta\mu_{\rm Na}$ = -1.78, $\Delta\mu_{\rm K}$ = -1.99, $\Delta\mu_{\rm N}$ = -2.40
MgTe	$\Delta\mu_{\rm Na}$ = -1.57, $\Delta\mu_{\rm K}$ = -1.77, $\Delta\mu_{\rm N}$ = -3.41
GaSe	$\Delta\mu_{\rm Zn}$ = -2.16, $\Delta\mu_{\rm P}$ = -0.19
GaTe	$\Delta\mu_{\rm Zn}$ = -0.38, $\Delta\mu_{\rm N}$ = -4.40
Al_2Se_3	$\Delta\mu_{\rm Mg}$ = -2.48, $\Delta\mu_{\rm N}$ = -4.30
BeTe	$\Delta\mu_{\rm Li}$ = -1.57, $\Delta\mu_{\rm Na}$ = -1.57, $\Delta\mu_{\rm N}$ = -5.29
GeS	$\Delta\mu_{\rm Na}$ = -1.77, $\Delta\mu_{\rm N}$ = -2.58

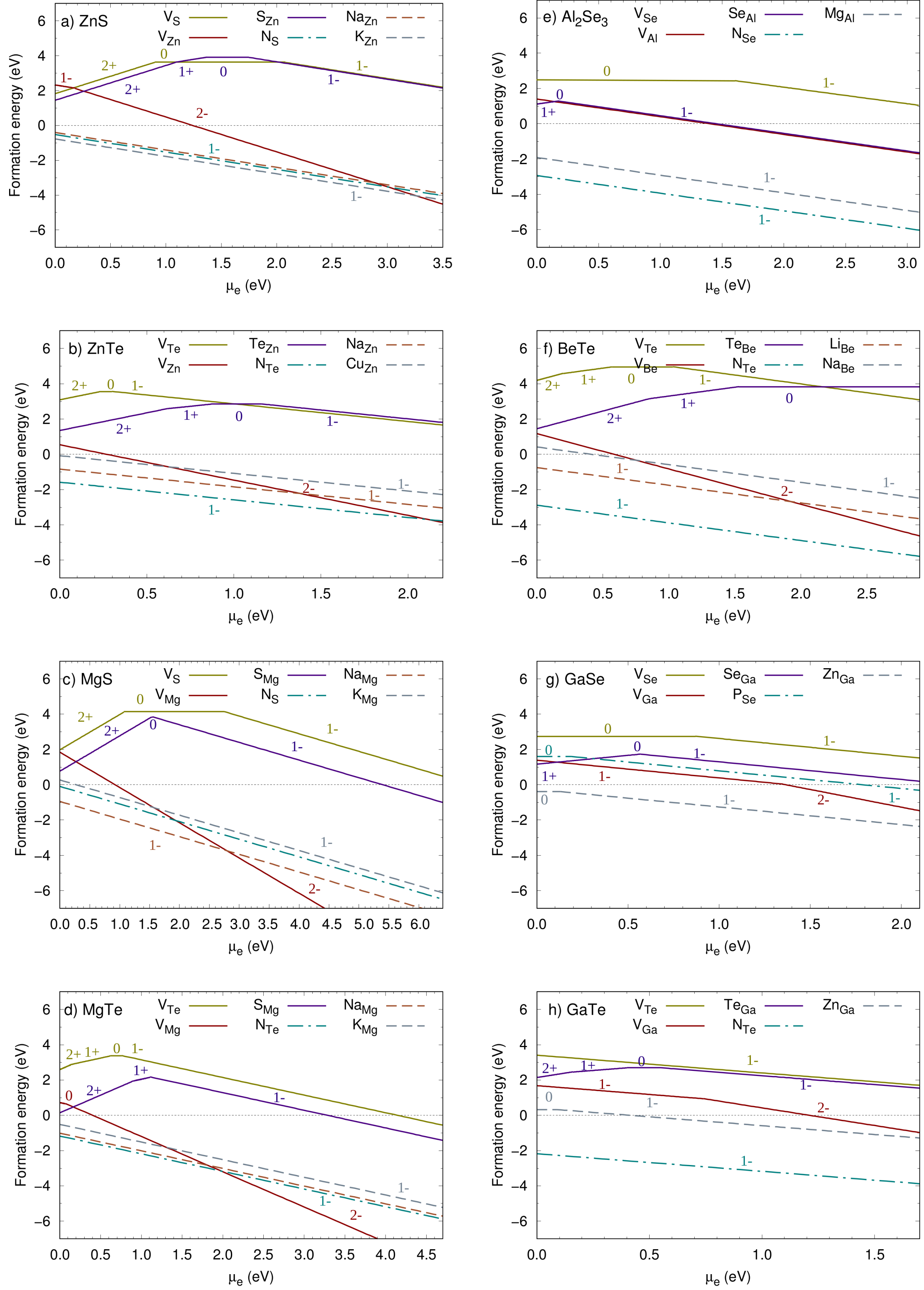

Figure 1: Defect formation energies in various non-oxide binary semiconductors as a function of electron chemical potential (μ_e) under anion-rich conditions. The formation energies are calculated for the extreme case when dopants are in the elemental phase.

2 ZnSe

The properties of ZnSe falls between that of ZnS and ZnTe (Figure 2). There are several reports on the good conductivity of p-doped ZnSe and our results agree well with the reported observations. In addition to Li, we found that Na can also increase the hole concentration in ZnSe.

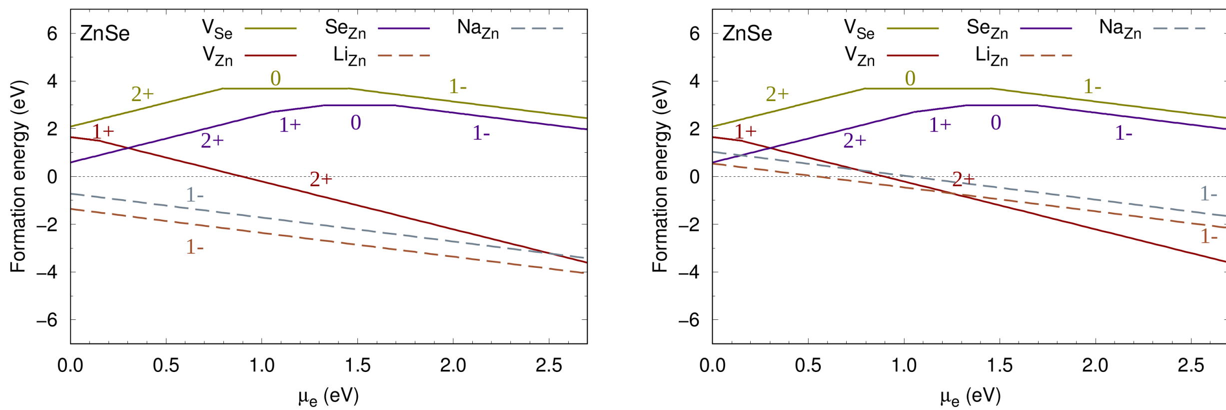

Figure 2: Defect formation energies in ZnSe as a function of electron chemical potential. Two extreme limits for chemical potential of dopants are shown. The left panel shows the formation energies when the dopants are in the elemental phase. The right panel shows the formation energies when the chemical potential of dopants are bounded by avoiding the formation of the secondary phases.

3 Role of the layer thickness

Changes in the hole effective masses with the layer thickness are shown in Table 3. As an example, here we show the modulation of the band gap of GeS with the layer thickness (Figure 3). Reducing the layers of GeS widened the band gap and at the same time induced a direct to indirect band gap transition. We studied the dopability and formation of extrinsic defects in GeS. In GeS, cation vacancies had lower formation energies than anion vacancies and antisites (Figure 4). The Na_{Ge} and N_S defects were found to increase the hole concentration in GeS.

Table 3: Hole effective masses for the bulk and monolayer of the selected layered compounds.

Compound	$m_h^*(m_e)$	
	Bulk	Monolayer
SnS	0.22	0.21
SnSe	0.19	0.15
GeS	0.91	0.71
GeSe	0.37	0.14
GeTe	0.15	0.14
GaTe	0.14	0.13

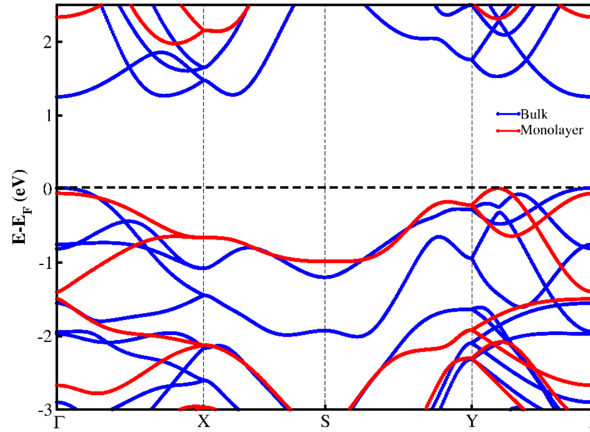

Figure 3: Changes in the electronic structure of GeS from bulk (blue curve) to monolayer (red curve).

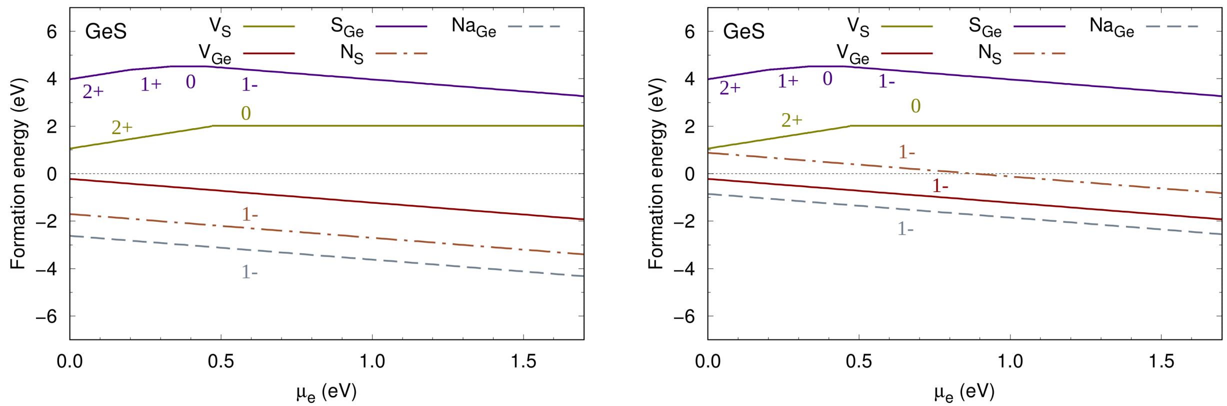

Figure 4: Defect formation energies in GeS as a function of electron chemical potential. Two extreme limits for chemical potential of dopants are shown. The left panel shows the formation energies when the dopants are in the elemental phase. The right panel shows the formation energies when the chemical potential of dopants are bounded by avoiding the formation of the secondary phases.

4 Band structures

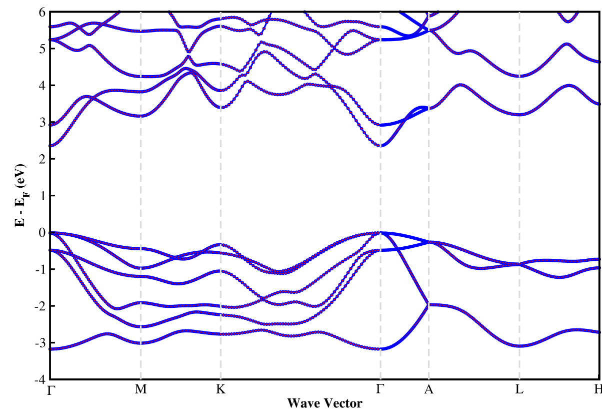

Figure 5: Band structure of MgTe calculated by PBE functional.

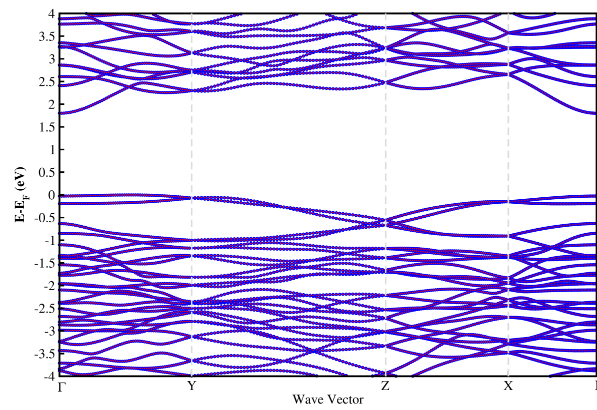

Figure 6: Band structure of Al_2Se_3 calculated by PBE functional.